Received: 29 September 2021 | Revised: 10 November 2021 | Accepted: 14 November 2021

DOI: 10.1002/mmce.22996

RESEARCH ARTICLE

INTERNATIONAL JOURNAL OF RF AND MICROWAVE COMPUTER-AIDED ENGINEERING WILEY

Development of a 70–110 GHz silicon corrugated horn for cosmic microwave background experiment

Zhao Feng[1,2] | Jia-Ning Li[2] | Zheng-Wei Li[2] | Yu-Peng Xu[2] | Cong-Zhan Liu[2] | Jin Fan[3] | Shi-Bo Shu[4] | Guan-Hua Gao[2] | Yi-Fei Zhang[2] | Xue-Feng Lu[2] | Xu-Fang Li[2] | Fang-Jun Lu[2] | Ai-Mei Zhang[2] | Yu-Dong Gu[2] | Yu Xu[2] | He Xu[2] | Di Wu[2] | Ying Wang[2]

[1]School of Microelectronics, University of Chinese Academy of Sciences, Beijing, China

[2]The Institute of High Energy Physics of the Chinese Academy of Sciences, Beijing, China

[3]The National Astronomical Observatories of the Chinese Academy of Sciences, Beijing, China

[4]California Institute of Technology, Pasadena, California, USA

Correspondence
Zheng-Wei Li and Cong-Zhan Liu, The Institute of High Energy Physics of the Chinese Academy of Sciences, 19B Yuquan Road, Shijingshan District, Beijing 100049, China.
Email: lizw@ihep.ac.cn (Z.-W. L.) and liucz@ihep.ac.cn (C.-Z. L.)

Jin Fan, The National Astronomical Observatories of the Chinese Academy of Sciences, Beijing 100101, China.
Email: jfan@bao.ac.cn

Funding information
National Natural Science Foundation of China, Grant/Award Numbers: 11653004, 11673024; Scientific Instrument Developing Project of the Chinese Academy of Sciences, Grant/Award Number: YJKYYQ20190065; Strategic Priority Research Program of the Chinese Academy of Science, Grant/Award Number: XDB23020000

Abstract

Next generation cosmic microwave background (CMB) polarization telescope will use large arrays of receiver with nearly 100 000 transition edge sensor (TES) detectors and receiving antennas. Such large TES and antenna array is a big challenge for the fabrication of TES and antennas. A 35-layers silicon-platelet corrugated horn for 70–110 GHz is designed and fabricated based on the micro electro mechanical system (MEMS) technology. Compared with the traditional corrugated horn, the last layer of the 35-layers silicon-platelet is designed with no corrugation to increase the beam symmetry. A parametric HFSS model of the horn was established to evaluate the performance of the horn and effect of fabrication process. The measured S11 and cross-polarization of the fabricated prototype horn are both below −20 dB while the sidelobe at 70 and 90 GHz is below −20 dB. The beam symmetry of the horn is good in 70–110 GHz band. The measured gain is greater than 15 dBi. These results show that the performance of the designed horn meets the requirement of CMB experiment.

KEYWORDS

cosmic microwave background (CMB), millimeter wave, corrugated horn, semiconductor fabrication

1 | INTRODUCTION

The cosmic microwave background (CMB) carries information about the early universe in the statistical properties of its polarization anisotropies. There are two complementary CMB polarization modes, called E and B modes. Especially, the B mode can be used to detect the primordial gravitational wave, which generated by the primordial tensor perturbations of the space–time metric. For this reason, the CMB B modes detection is one of the prime science targets of many CMB polarization experiments, just like BICEP2[1] and AliCPT.[2] For ground-based

CMB experiment, the CMB can only be observed in specific windows of atmospheric transmission. Photon noise from the atmosphere, and emission from fluctuating inhomogeneities of water vapor are dominated noise for the ground-based CMB experiment. This can be represented by the brightness temperature of the sky at certain frequency. Taken into consideration of the atmosphere transmittance and sky brightness, the observable windows for ground-based CMB experiment are 35, 90, 150, and 220 GHz.[3] For the primordial B modes polarization, there are foreground contaminations dominated by the synchrotron and dust emission from the galactic interstellar medium. The contamination is at a minimum relative to the CMB around 60–100 GHz.[4]

The receiver's performance determines the sensitivity of the CMB telescope. One of the important performances for the receiver is the beam map, cross-polarization, and bandwidth of the feed antenna. The asymmetry of the beam map and bad cross-polarization will induce E-mode polarization leakage into B-mode polarization. This will reduce the sensitivity of the CMB polarization telescope.[5] Three kinds of feed antennas have been used in CMB experiments. The lenslet-coupled sinuous antenna, which gives high gain, high coupling efficiency, and very broad bandwidth, has been used in Polarbear-2 and SPT-3G experiments.[6,7] But, this kind of antenna requires a high-accuracy elliptical lens alignment and its polarization axis depends on the frequency. The double-slot dipole antennas and slot array, which give low cross-polarization, have been used in the Polarbear-1 and BICEP3.[8,9] However, these antennas give higher sidelobe. And it's hard to increase its relative bandwidth, which limit its use in multifrequency CMB telescope. The double-slot antenna requires a lenslet which is similar to sinuous antenna to increase the gain. The highly beam symmetry requirement will increase the design and fabrication complex for the slot array with a feed network. Another alternative feed antenna is corrugated horn, which is used in ACTPol and SPTpol telescope.[10–12] Compared with other two kinds antenna, corrugate horns have lower sidelobe and highly symmetric beams and low cross-polarization. And the corrugated feedhorn can be designed as broadband antenna, which can be used in multifrequency CMB telescope. These benefits of the corrugate feedhorn make it as a novel antenna for the CMB telescope.[5]

The traditional fabrication methods of corrugated horns are machining and electroforming. Direct machining requires special tools for small corrugations and is time consuming for fabricating a large horns array.[13] At the same time, it is very difficult for direct machining to fabricate a nonlinear profile and ring-road corrugated horn when the size of the horn is getting smaller in high frequency band. Electroforming requires high-accuracy complementary mandrels for every corrugated horn, which causes high cost when fabricating the large horn array.[14] These two methods are not suitable for the next-generation CMB projects, which require hundreds of pixels in a single module and nearly 100 000 pixels in total.[5] To meet this requirement, silicon stacked horn array by microfabrication technology is state of the art.[10–14] In this approach, the profile of a corrugated horn is separated into several layers at each corrugation position. The pattern of each layer is defined on several Si platelets by photolithography and deep reactive ion etching (DRIE). After etching, the Si platelets is coated with a metal layer. And then Si wafers are stacked into a horn array. The corrugated horn assembled with Si wafers has similar performance with the horn fabricated by machining.[13–15] The use of silicon largely decreases the weight of horns, which lowers the required cooling power on the focal plane. Also, the same material to make the horn and detector array module is beneficial to reduce the integration complexity caused by the difference in thermal expansion coefficients of metal and silicon.[16] An 84 pixels horn array consisting of 33 Si wafers was fabricated by NIST in 2010 and an array with 507 horns was fabricated in 2016.[17–19] The sidelobe and cross-polarization of these horn are below −20 dB. The ring-loaded corrugated horn fabricated by NIST[10] shows low sidelobes, low cross-polarization, and good symmetry of the beam. To increase the bandwidth of the feedhorn, the primary silicon platelet stacked feedhorn of NIST is designed with a ring-load structure. This increases the complexity of fabrication and integration. A smooth-profile feedhorn was investigated by NIST to replace the ring-load corrugated feedhorn. This simplified the fabrication process but increase the difficulty of design. A 37-element array was fabricated by Mandelli et al.[20] This array was made by aluminum using chemical etching and computer numerical control (CNC) milling technology. The return loss of chemically etched corrugated feedhorn is below −25 dB, and the cross-polarization is below −20 dB. For 500–750 GHz band, a stacked corrugated horn was made by Zhao et al.[21] The sidelobe of this horn is below −20 dB and the gaussicity of beam is higher than 95%. But these two kinds of horn described above are not fabricated with silicon, that will cause the mismatch of thermal expansion coefficients between metal and silicon.

In this article, a 35-layer sine-squared profile corrugated horn for 70–110 GHz was investigated by stacking silicon platelets. To optimize the beam symmetry, one additional layer without corrugation was added to the primary designed 34 layers sine-squared profile corrugated. A parametric HFSS model of the designed 35 layers

corrugated feedhorn was constructed to evaluate the effect of the fabrication accuracy. Based on the simulation result, the fabrication process of the feedhorn was optimized to simplify the fabrication used by NIST.[19] This single horn design serves as a pathfinder for future large arrays. The return loss, beam patterns, and cross-polarizations have been measured. The difference between design and measurements has been analyzed and discussed.

2 | GEOMETRY AND DESIGN PROCEDURE

2.1 | Design of a 70–110 GHz silicon corrugated horn

The designed horn should have a highly symmetric beam to achieve a good common-mode rejection performance in the target band. First of all, we should define a suitable horn profile with optimized corrugations. Finally, a sine-squared profile was chosen, shown in Figure 1. Compared with linear profile design, sine-squared profiles can reduce the volume and corrugation needed in the horn, this can simplify the fabrication of the corrugated horn.[22] At the same time, smaller volume can reduce the thermal resistance, this makes it easier to control the temperature of horn in cryogenic situation.

The inner profile of the horn is defined by[23]

$$R_j = R_i + (R_o - R_i)\left[(1-A)\frac{j-1}{N-1} + A\sin^2\left(\frac{\pi}{2}\frac{j-1}{N-1}\right)\right] \quad (1)$$

In formula (1), A is a variable parameter between 0 and 1 which is used to control the curvature of corrugated horn. R_i and R_o are the input radius and output radius, respectively. The N and j are the total number of platelet and the number of j-th platelet. The total number of platelets for the designed horn is 35.

The most important parameter that influence the beam pattern of the horn is the slot depth (d), shown in Figure 1. In general, the slot depth ranges from approximately $\lambda/2$ to $\lambda/4$ in the first several slots. These slots serve as a mode-converter which is used to match the impedance of the circular waveguide and the feed horn. This converter transforms TE11 mode in circular waveguide to HE11 mode.[18] The HE11 mode gives a highly symmetric beam pattern. In this article, the horn's first six slots are defined as mode-converter, the depth of these slots are defined by the formula below[23]:

$$d_j = \left\{\sigma - \frac{j-1}{N_{\mathrm{mc}}}\left(\sigma - \frac{1}{4}\exp\left[\frac{1}{2.114\left(kR_j\right)^{1.134}}\right]\right)\right\}\lambda \quad (2)$$

where σ is a percentage factor ranges from 0.4 to 0.5. The N_{mc} is the total number of slots serving as a mode-converter. The k_c is the number of wave and the R_j is the radius of the profile. The percentage factor is optimized to be 0.42. The λ is chosen to be the wavelength in 87.7 GHz after optimization. This achieves a better performance of beam symmetry at center frequency of the horn.

The depth of rest slots is defined by the formula below:

$$d = k\frac{\lambda}{4} \quad (3)$$

where k is a modified coefficient related to the inner profile radius.[23,24] To have a better performance at low frequency, a correction item d_s is added to d. Then, the total slot depth is given by:

$$d_j' = d + d_s \quad (4)$$

d_s is optimized to be 0.1 mm.

The horn length has an impact on the sidelobe performance.[23] The length is usually chosen to be $5^*\lambda_c$ (center frequency wavelength) or longer,[22] which can achieve a sidelobe less than −20 dB.[25] At the same time, it is demonstrated that there should be four corrugations per λ_c at least.[22] Besides, the thickness of each platelet is usually chosen to be range from $\lambda_c/10$ to $\lambda_c/5$.[23] In consideration of these factors mentioned above and the center frequency of the horn (90 GHz), each platelet's thickness (p) (shown in Figure 1) is chosen to be 525 μm. The total length of the horn is 18.375 mm with 35 platelets and 34 corrugations. There are six slots per λ_c. The pitch-to-width ratio (t/p) (shown in Figure 1) should be 0.7–0.9, but for a wide-band, it can be chosen to be 0.5–0.9.[22,23] The slot width (t) (shown in Figure 1) is optimized to 330 μm and the pitch-to-width ratio is about 0.629.

The output radius (R_o) of the horn is determined by the radiation angle of the CMB telescope, and gain of the corrugated horn. The radiation angle of designed horn is

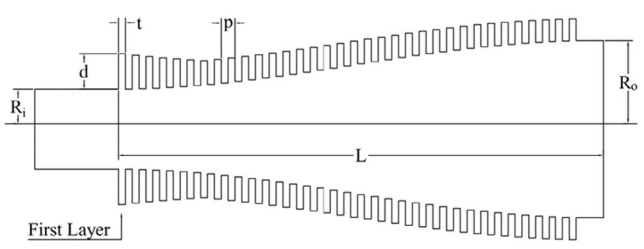

FIGURE 1 The profile of the designed corrugated horn

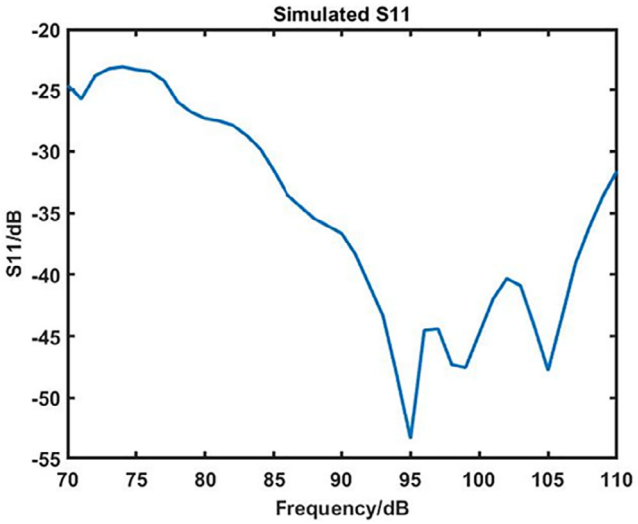

FIGURE 2 The optimized return loss

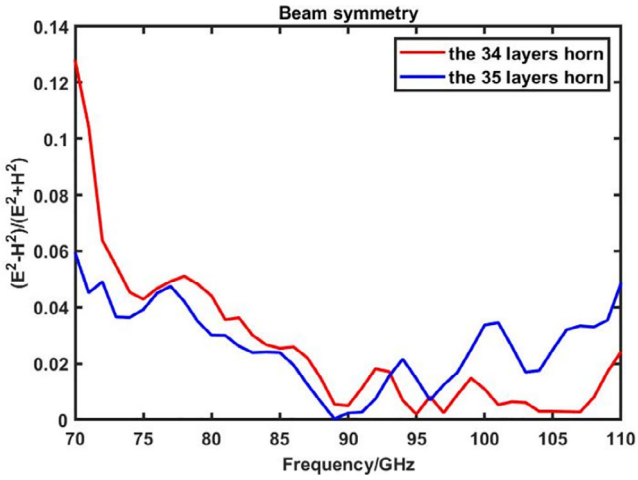

FIGURE 3 Simulation result of beam symmetry

set at 18° at 90 GHz. Within a certain frequency range, larger output radius will have higher gain and narrower beam width. The input radius R_i is determined by the wavelength at 70 GHz. Simulated by HFSS, the output radius is optimized to 4.506 mm and the input radius is optimized to 1.633 mm, which achieves an in-band gain of 15 dBi and in-band return loss of −20 dB. The simulation result of return loss is shown in Figure 2.

A function is used to assess the beam symmetry of the corrugated horn[18]:

$$P = \sum_{\theta=0}^{\theta=\theta_{\text{stop}}} \frac{(E^2 - H^2)}{(E^2 + H^2)} \tag{5}$$

In formula (5), E and H is the amplitude of E-plane and H-plane, and θ_{stop} is the cold stop angle of the horn, which is 18°. Our target of symmetry parameter is below 0.1, which could meet the requirement of systematic error for B mode detection.[26] The last layer of corrugated horn has the same radius to the 34th platelet and has no slot in order to make a complete corrugation in the 34th layer. Simulation result shows that the beam symmetry in low frequency band has a better performance than the horn without the last layer. The simulation result of symmetry parameter P at different frequency is shown in Figure 3. It is shown that the symmetry parameter P is below 0.06. The parameters of designed horn are shown in Table 1.

TABLE 1 Parameters of designed horn

Parameter	Value (mm)	Parameter	Value (mm)
R_i	1.633	L	0.6
R_o	4.509	d_1	1.537
p	0.525	d_{34}	0.952
t	0.33		

2.2 | Fabrication of a single Si corrugated horn

Commercial 4-in. Si wafers with thickness of 525 ± 10 μm are used. To simplify fabrication process, both the inner profile pattern and the corrugation pattern are fabricated on a single Si platelet. Therefore, each wafer will be etched twice with different depth. In total, the 35 layers of the single pixel corrugate horn are fabricated on four silicon wafers. The fabrication process is shown in Figure 4. We first deposit a 4-μm thick SiO_2 layer by using plasma enhanced chemical vapor deposition (PECVD). The deposited SiO_2 is used as the mask for the second DRIE process. The pattern on this SiO_2 layer is defined by contact lithography and dry etching. Then we use the same lithography process to define the inner profile pattern and etch away 280 μm Si using DRIE. After removing the photoresist, a second DRIE is done with a depth of 330 μm. The measured verticality of DRIE process is about 89°. The remaining SiO_2 is removed by BOE wet etching. Before electroplating, a seed layer (Ti: Au = 20:200 nm) is sputtered on both sides of the wafer. Finally, both sides of the wafer are electroplated with 1.5-μm thick Au, which is much thicker than the skin-effect depth at 90 GHz (0.28 μm). The recipes of the fabrication process are shown in Table 2.

We checked the cross section of the fabricated wafer using scanning electron microscope (SEM) and an extra step-like structure is found at the edge of the inner profile, shown in Figure 5. The sharp edge suggests that there might be some photoresist residue left on top of this

FIGURE 4 Fabrication process

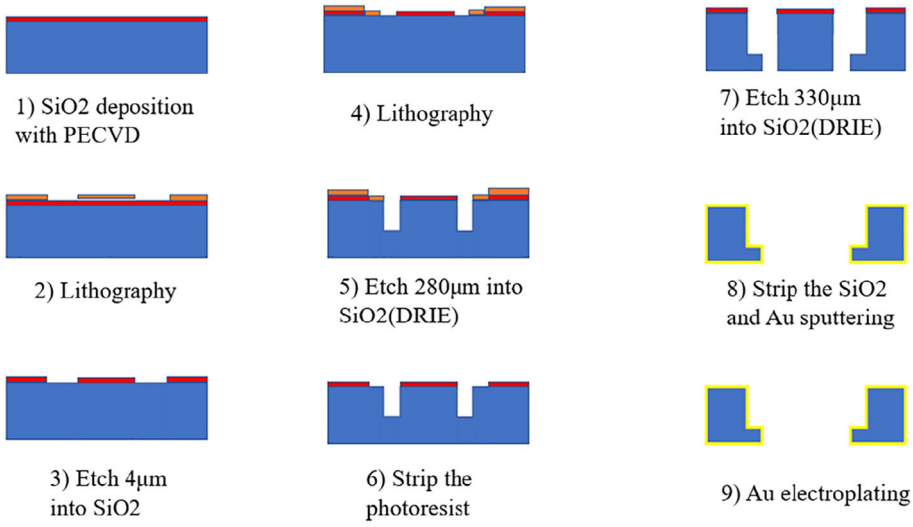

TABLE 2 Recipe of fabrication process

Description	Process	Value (μm)	Description	Process	Value (μm)
SiO_2 deposition	PECVD 350°C 1.4 Torr SiH4:12sccm N2O:700sccm 2250s	4	*Si etching*	DRIE, RF1650W SF6:450sccm C4F8:200sccm	−280
Lithography	Photoresist: AZ4620 1000 r/min 30s EVG5200	12	*Au sputtering*	Magnetron sputtering	0.2
SiO_2 etching	NLD-570 CF4:40sccm RF: 1000/150 W 12 min	−4	*Au electroplating*	60°C Current 30 mA 45 min	1.5

structure, blocking Si etching.[27] We found that the effect of this extra step structure is negligible, after simulating in HFSS.

After dicing, 35 platelets are stacked together using two alignment pins with diameters of 2 mm. Then we apply Stycast 2850 FT glue around the platelet for connecting. The alignment pin has a negative tolerance of 6 μm, so we expect the alignment accuracy is better than 10 μm. Two M2.5 holes are used for screws, connecting a customized circular-to-rectangular waveguide transition. Compared to the fabrication process of NIST,[19] the horn is not electroplated after being stacked. This can simplify the process of the fabrication but will form gaps between platelets. Two 1-μm thick gaps are set between the first two layer and between 17th and 18th layer to estimate the effect of gap in different positions. The simulation shows negligible impact on performances of beam symmetry (shown in Figure 6).

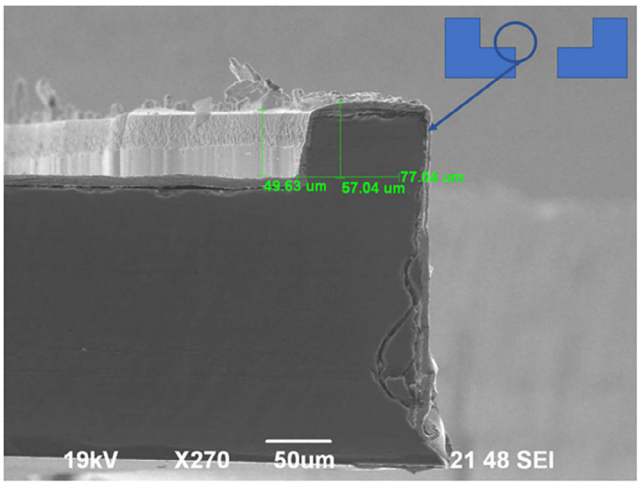

FIGURE 5 SEM image of the cross section of extra step structure at the corner of etched slot

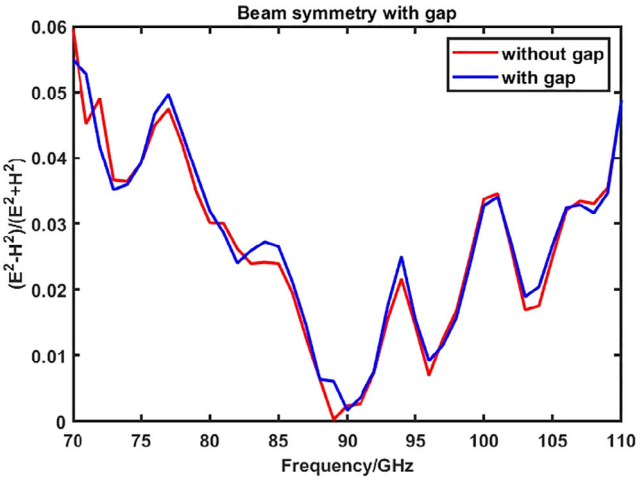

FIGURE 6 Simulation of beam symmetry with fabrication tolerance

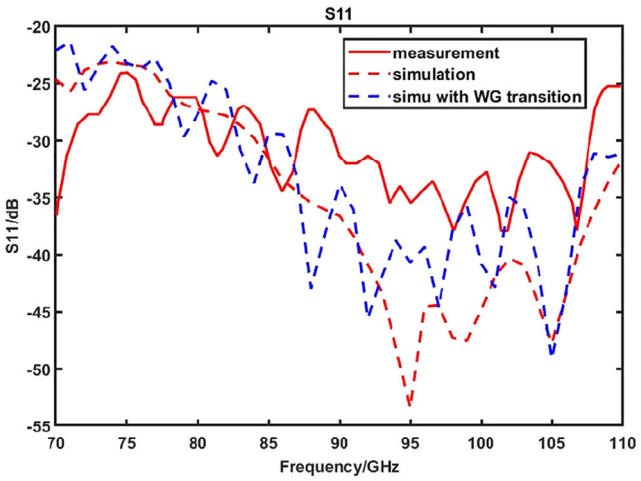

FIGURE 8 Measured S11 of the fabricated prototype at different frequency

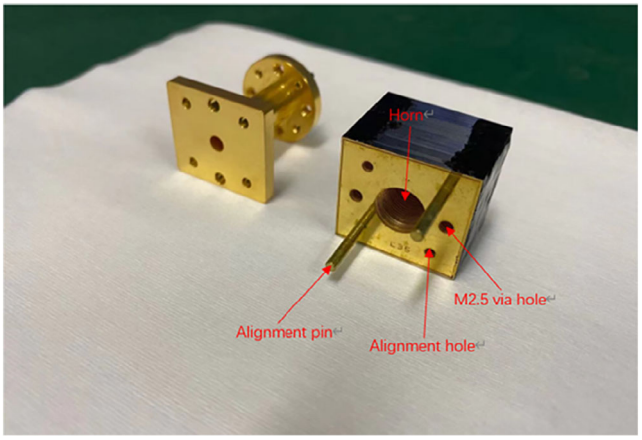

FIGURE 7 Fabricated waveguide transition (left in the photon) and corrugated horn (right in the photo)

The assembled horn and the waveguide transition are shown in Figure 7.

3 | PROTOTYPE AND MEASUREMENT

The measured S11, shown in Figure 8, is below −24 dB in 70–110 GHz frequency band, including the transition waveguide. In low frequency band, the measured S11 agrees with the simulation. For frequency higher than 85 GHz, the S11 is limited by the transition waveguide, according to the shape of the simulated S11.

The far-field beam mapping was measured between 70 and 110 GHz. The frequency multiplication module was used to extend the measurement frequency band. A signal generator and a standard gain horn antenna are used as transmitter for far-field measurements. A spectrum analyzer is used to measure the signal received by the antenna under test (AUT). Before measuring the fabricated horn, a standard gain horn antenna is used as a receiver for gain calibration. Then the fabricated Si horn is placed as the receiver and alignment between two antennas are performed. The rotating platform of the AUT, rotated ±90° during measurement in order to measure the directivity in different angle. To measure the *E*-plane and *H*-plane beam patterns of the horn, the polarizations of two antennas are aligned and the AUT rotates in parallel and perpendicular to the standard antenna. Besides, the polarization of the standard horn rotates 90° to the polarization of the AUT to measure cross-polarization.[19] The distance of two antennas meets the far-field requirement. All measurements are carried out in a Microwave Anechoic Chamber. The measurement setup is shown in Figure 9.

The co-polarization, cross-polarization, and beam symmetry results in 70–110 GHz are shown in Figure 10. The main lobes of 70, 80, 90, and 100 GHz are in consistent with the simulation. Meanwhile, the sidelobe at 70–110 GHz is below −20 dB, which meets the expected target. The *E*-plane at 110 GHz shows lower sidelobe and broader beamwidth comparing to simulation result. We remeasured the beam pattern at 110 GHz in another laboratory. The result of remeasurement shows that the main lobe at 110 GHz is in consistent with simulation. The higher level of sidelobe is related to gaps between the stacked platelets. It is found that the remeasured *E*-plane beam pattern at 110 GHz shows agreement with the simulation after considering gaps between the stacked platelets. The ripples may be related to the systematical error.

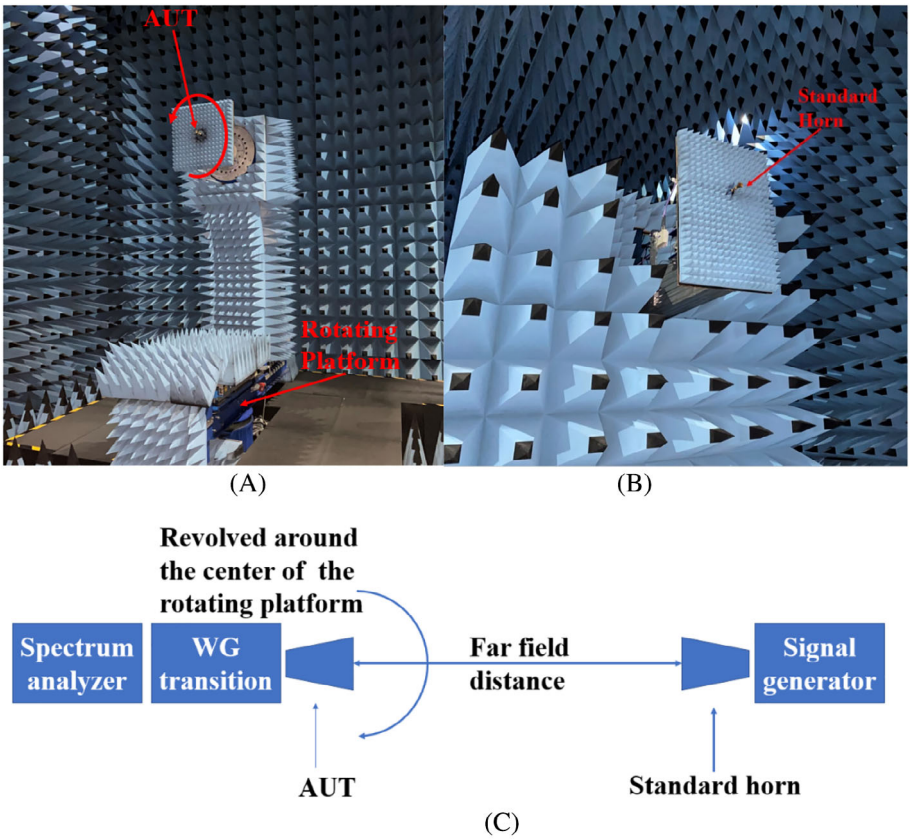

FIGURE 9 AUT and far-field measurement system. (A) The AUT. (B) Standard Horn. (C) Schematics of polarization measurement system

The measured cross-polarization is below −20 dB in 70–110 GHz, but the measured cross-polarization is 20 dB higher than simulations. The higher level of cross-polarization is related to the manufacturing error of wave-guide transition, which cause the leakage of the co-polar beam patterns at the measurement plane of the cross-polarization.[19] It is demonstrated that the misalignment between the different layers of the horn also causes higher cross-polarization.[20] The cross-polarization at 70 GHz has the similar beam shape to the main lobe, which indicates that the polarization of the AUT is not orthogonal to the polarization of the standard gain antenna when measuring the polarization. The asymmetry of cross-polarization is most likely a result from the defect in the horn.

The beam symmetry parameter at low frequency band shows agreement with simulation result. The higher symmetry parameter at 90 GHz is related to the misalignment between the centers of two horns. The symmetry parameter at 110 GHz is much higher than simulation, after remeasuring, the symmetry parameter shows agreement with simulation result.

To measure the gain of the AUT, another standard gain antenna is used. The maximum received power of AUT is measured as P_x first. The standard gain antenna replaces the AUT to measure its maximum received power as P_s. The gain of standard antenna is G_s, then the gain of AUT can be calculated by:

$$G_x = G_s + (P_x - P_s) \tag{6}$$

The gain at 70, 90, and 110 GHz is 15.8,16.9, and 18 dBi, respectively, while the simulation results are 15,17.4, and 19.5 dBi (as shown in Figure 11).

The measured in-band gain has the same tendency with the measured S11. In low frequency band, the measured gain is higher than the simulation. The reason is that the cut-off frequency of the standard gain antenna used for the gain measurement is 73.8 GHz, and the performance of the standard horn at 70 GHz is not calibrated, which causes the measurement error. In high frequency, the measured gain is less than the simulation, which is caused by the loss of the frequency multiplication module and the defect in the transition.

We compare our work with other stacked horns in the past few years in Table 3. The comparison shows that the performance of our horn can reach the same level as other studies. Besides, the last step of fabrication process is simplified comparing to the process from NIST, which shows negligible impact on the beam symmetry. To optimize the beam symmetry in low frequency band (70–90 GHz), we add a non-corrugation structure in 35th

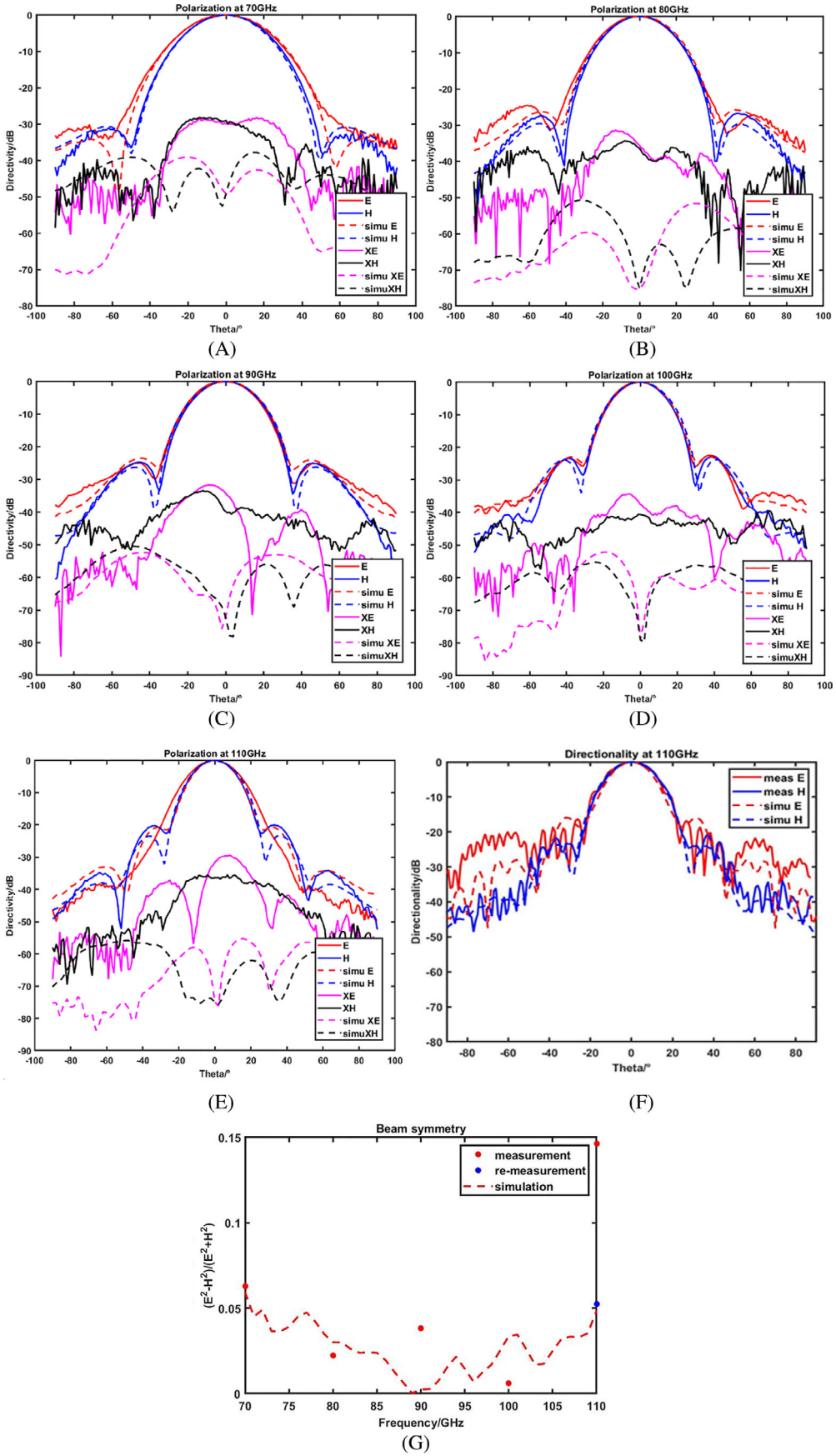

FIGURE 10 Measured beam pattern and cross-polarization at 70, 90, and 110 GHz. (A) Beam pattern at 70 GHz; (B) beam pattern at 80 GHz; (C) beam pattern at 90 GHz; (D) beam pattern at 100 GHz; (E) beam pattern at 110 GHz; (F) remeasured beam pattern at 110 GHz; (G) beam symmetry parameters

TABLE 3 Comparison with other works

	Bandwidth	Cross-pol	Side lobe	RL
Datta et al.[10]	2.5:1	<−20 dB	<−20 dB	/
Simon et al.[18]	2.37:1	<−17.7 dB	<−15 dB	<−10 dB
Britton et al.[19]	1.5:1	<−23 dB	<−25 dB	<−13 dB
Mandelli et al.[20]	1.21:1	<−20 dB	<−25 dB	<−25 dB
Zhao et al.[21]	1.21:1	<−40 dB	<−20 dB	<−9.5 dB
Our work	1.57:1	<−28.2 dB	<−20 dB	<−24 dB

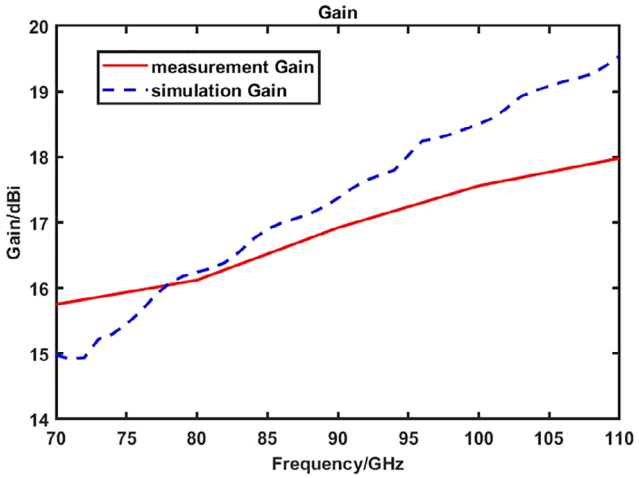

FIGURE 11 Gain of the designed horn

layer of the horn. The simulation and measured result shows that the beam symmetry is better after adding 35th layer.

4 | CONCLUSION

In this article, a 70–110 GHz 35 layers sin-squared profile corrugated horn is designed and fabricated. Simulation shows that the horn has a good performance of beam symmetry with a non-corrugation structure in the 35th layer.

The measured S11 of the fabricated feed horn prototype is below −24 dB. The cross-polarization of the horn is below −20 dB. The sidelobe in 70–100 GHz is below −20 dB, and the gain of the horn is larger than 15 dBi in coverage frequency band. The design is also simplified comparing smooth-profile feedhorn. The measurement result shows that the designed horn can meet the requirements of CMB experiment.

DATA AVAILABILITY STATEMENT

The data that support the findings of this study are available from the corresponding author upon reasonable request.

ORCID

Jin Fan https://orcid.org/0000-0002-4482-0196

REFERENCES

1. Ade PAR, Aikin RW, Barkats D, et al. Detection of b-mode polarization at degree angular scales by BICEP2. *Phys Rev Lett*. 2014;112(24):241101.
2. Salatino M, Austermann JE, Thompson KL, et al. The design of the ALI CMB polarization telescope receiver. SPIE Astronomical Telescopes + Instrumentation; 2020.
3. Errard J, Ade PAR, Akiba Y, et al. Modeling atmospheric emission for CMB ground-based observations. *Astrophys J*. 2015; 809(1):63.
4. Delabrouille J, Cardoso JF. Diffuse source separation in CMB observations. *Data Anal Cosmol*. 2008;665:159-205.
5. Abitbol MH, Zeeshan A, Darcy B, et al. CMB-s4 technology book[M/OL]. 1st ed. arXiv:1706.0246; 2017
6. Edwards JM, O'Brient R, Lee AT, Rebeiz GM. Dual-polarized sinuous antennas on extended hemispherical silicon lenses. *IEEE Trans Antenna Propag*. 2012;60(9):4082-4091.
7. O'Brient R, Ade P, Arnold K, et al. A dual-polarized broadband planar antenna and channelizing filter bank for millimeter wavelengths[J]. *Appl Phys Lett*. 2013;102(6):1-24.
8. Arnold K, Ade PAR, Anthony AE, et al. The bolometric focal plane array of the polarbear CMB experiment. SPIE Astronomical Telescopes + Instrumentation; 2012.
9. Hui H, Ade PAR, Ahmed Z, et al. Bicep3 focal plane design and detector performance. SPIE Astronomical Telescopes + Instrumentation; 2016.
10. Datta R, Hubmayr J, Munson C, et al. Horn coupled multichroic polarimeters for the atacama cosmology telescope polarization experiment. *J Low Temp Phys*. 2014;176(5):670-676.
11. Britton J, Yoon KW, Beall JA, et al. Progress toward corrugated feed horn arrays in silicon. AIP Conference Proceedings; 2009: 1185.
12. Mcmahon J, Beall J, Becker D, et al. Multi-chroic feed-horn coupled TES polarimeters. *J Low Temp Phys*. 2012;167(5–6): 879-884.
13. Sekiguchi S, Sugimoto M, Shu S, et al. Broadband corrugated horn array with direct machined fabrication. *IEEE Trans Terahertz Sci Technol*. 2017;7(1):1-6.
14. Beniguel Y, Berthon A, Klooster CV, Costes L. Design realization and measurements of a high performance wide-band corrugated horn. *IEEE Trans Antenna Propag*. 2005;53(11): 3540-3546.
15. Vishnu GJ, Pujara DA, Pandya H. Design and development of a d-band corrugated horn antenna for millimeter-wave plasma diagnostics. *Prog Electromag Res Lett*. 2019;85:101-108.

16. Ward JT, Austermann J, Beall JA, et al. Mechanical designs and development of TES bolometer detector arrays for the advanced ACTPol experiment. SPIE Astronomical Telescopes + Instrumentation; 2016.
17. Nibarger JP, Beall JA, Becker D, et al. An 84 pixel all-silicon corrugated feedhorn for CMB measurements. *J Low Temp Phys*. 2012;167(3–4):522-527.
18. Simon SM, Austermann J, Beall JA, et al. The design and characterization of wideband spline-profiled feedhorns for advanced ACTPol. SPIE Astronomical Telescopes + Instrumentation; 2016.
19. Britton JW, Nibarger JP, Yoon KW, et al. Corrugated silicon platelet feed horn array for CMB polarimetry at 150 GHz. SPIE Astronomical Telescopes + Instrumentation; 2010.
20. Mandelli S, Manzan E, Mennella A, et al. A chemically etched corrugated feedhorn array for D-band CMB observations. *Exp Astron*. 2020;51:249-272.
21. Zhao J, Liu Z, Liu Y, Lu H, Cheng C, Lv X. Metallic micromachined corrugated conical horn antenna in the 500–750 GHz band. 2021 IEEE MTT-S International Wireless Symposium (IWS); 2021:1-3
22. Olver AD, Clarricoats PJ, Kishk AA, Shafai L. *Microwave Horns and Feeds*. The Institute of Electrical Engineers; 1994.
23. Granet C, James GL. Design of corrugated horns: a primer. *IEEE Antenna Propag Mag*. 2005;47(2):76-84.
24. Milligan TA. *Modern Antenna Design*. 2nd ed. John Wiley & Sons; 2005.
25. Clarricoats PJB, Olver AD. *Corrugated Horns for Microwave Antennas*. Peter Peregrinus; 1984.
26. Shimon M, Keating B, Ponthieu N, Hivon E. CMB polarization systematics due to beam asymmetry: impact on inflationary science. *Phys Rev D*. 2008;77(8).
27. Yan J. *Micro and Nano Fabrication Technology*. Springer Nature Singapore; 2018.

How to cite this article: Feng Z, Li J-N, Li Z-W, et al. Development of a 70–110 GHz silicon corrugated horn for cosmic microwave background experiment. *Int J RF Microw Comput Aided Eng*. 2022;32(3):e22996. doi:10.1002/mmce.22996